Biomedical Research (Tokyo) **38** (2) 123–134, 2017

Histochemical assessment for osteoblastic activity coupled with dysfunctional osteoclasts in *c-src* deficient mice

Hisashi Toraya[1], Tomoka Hasegawa[1], Naoko Sakagami[2], Erika Tsuchiya[1], Ai Kudo[1], Shen Zhao[1], Yasuhito Moritani[1], Miki Abe[1], Taiji Yoshida[1], Tomomaya Yamamoto[1], Tsuneyuki Yamamoto[1], Kimimitsu Oda[3], Nobuyuki Udagawa[4], Paulo Henrique Luiz de Freitas[5], Minqi Li[6], and Norio Amizuka[1]

[1] Department of Developmental Biology of Hard Tissue, Graduate School of Dental Medicine, Hokkaido University, Sapporo, Japan; Divisions of [2] Reconstructive Surgery for Oral and Maxillofacial Region and [3] Biochemistry, Niigata University Graduate School of Medical and Dental Sciences, Niigata, Japan; [4] Department of Biochemistry, Matsumoto Dental University, Shiojiri, Japan; [5] Department of Dentistry, Federal University of Sergipe at Lagarto, Brazil; and [6] Shandong Provincial Key Laboratory of Oral Biomedicine, The School of Stomatology, Shandong University, Jinan, China

(Received 25 November 2016; and accepted 6 January 2017)

ABSTRACT

Since osteoblastic activities are believed to be coupled with osteoclasts, we have attempted to histologically verify which of the distinct cellular circumstances, the presence of osteoclasts themselves or bone resorption by osteoclasts, is essential for coupled osteoblastic activity, by examining *c-fos*$^{-/-}$ or *c-src*$^{-/-}$ mice. Osteopetrotic *c-fos* deficient (*c-fos*$^{-/-}$) mice have no osteoclasts, while *c-src* deficient (*c-src*$^{-/-}$) mice, another osteopetrotic model, develop dysfunctional osteoclasts due to a lack of ruffled borders. *c-fos*$^{-/-}$ mice possessed no tartrate-resistant acid phosphatase (TRAPase)-reactive osteoclasts, and showed very weak tissue nonspecific alkaline phosphatase (TNALPase)-reactive mature osteoblasts. In contrast, *c-src*$^{-/-}$ mice had many TNALPase-positive osteoblasts and TRAPase-reactive osteoclasts. Interestingly, the parallel layers of TRAPase-reactive/osteopontin-positive cement lines were observed in the superficial region of *c-src*$^{-/-}$ bone matrix. This indicates the possibility that in *c-src*$^{-/-}$ mice, osteoblasts were activated to deposit new bone matrices on the surfaces that osteoclasts previously passed along, even without bone resorption. Transmission electron microscopy demonstrated cell-to-cell contacts between mature osteoblasts and neighboring ruffled border-less osteoclasts, and osteoid including many mineralized nodules in *c-src*$^{-/-}$ mice. Thus, it seems likely that osteoblastic activities would be maintained in the presence of osteoclasts, even if they are dysfunctional.

In a physiological state, bone formation is coupled with bone resorption during the process of normal bone remodeling, which continuously takes place along the surface of bone, with resorption preceding formation. Literally, osteoclastic bone resorption has been reported to trigger the differentiation and activation of osteoblasts, which is referred to as a "coupling phenomenon" (4, 10, 11, 13). Howard *et al.* had proposed the existence of a coupling factor enabling subsequent bone formation (17), and transforming growth factor beta (TGFβ) and insulin-like growth factor (IGF) were assumed to serve as a coupling factor by being released from bone matrix (7, 15, 16). Other cellular mechanism of cell coupling from osteoclasts to osteoblastic cells can be additionally hypothesized, *e.g.,* by mediating the secretion of coupling factors, or by binding of the membrane-bound coupling factors. However, it is

Address correspondence to: Tomoka Hasegawa, DDS, PhD
Department of Developmental Biology of Hard Tissue, Graduate School of Dental Medicine, Hokkaido University, Kita 13 Nishi 7 Kita-ku, Sapporo, 060-8586, Japan
Tel/Fax: +81-11-706-4226
E-mail: hasegawa@den.hokudai.ac.jp

still veiled which manners of cell coupling, release of coupling factors from bone matrix, or secretion and/or membrane-bound coupling factors would activate osteoblastic cells. Therefore, in order to provide a clue for understanding how osteoclasts couple with osteoblastic cells, it seems preferable to histologically examine the osteoblastic activities of mice in which osteoclasts are deficient or dysfunctional for bone resorption.

One of adequate animal models lacking osteoclasts is the *c-fos* deficient mice (*c-fos*$^{-/-}$ mice) (12), which is a strain characterized by osteopetrosis due to the absence of mature osteoclasts and their precursors (38): The lack of osteoclasts is ascribed to defective differentiation of hematopoietic precursors into osteoclastic lineage at a very early stage (8). *c-fos* is a member of the Fos family of genes that, with Jun proteins, form the activator protein-1 (AP-1) family of heterodimeric transcription factors (33). It acts as an essential switch between osteoclast and macrophage differentiation from a common progenitor, and osteoclasts do not form in the absence of c-Fos (38). c-Fos serves as a complex with c-Jun to regulate the expression of nuclear factor of activated T cells 2 (NFAT2), also referred to as NFATc1, in osteoclasts to mediate its osteoclastogenic effects. NFATs and AP-1 form complexes on the promoters of many genes, but the precise nature of this interaction in osteoclastogenic genes has yet to be identified.

c-src deficient mouse is another osteopetrotic model (34). Src family tyrosine kinases have a common domain organization, with each segment designated as a Src-homology (SH) region. The N-terminal segments include the SH4 domain, which is a myristoylation and membrane-localization signal, as well as a "unique" domain (25). Soriano *et al*. had reported that targeted disruption of the *c-src* gene in mice (*c-src*$^{-/-}$ mice) induced osteopetrosis, a disorder characterized by decreased bone resorption, without showing any obvious morphological or functional abnormalities in other tissues or cells (34). The osteopetrotic phenotype of *c-src* disrupted mice is cell autonomous and occurs in mature osteoclasts: *c-src*$^{-/-}$ osteoclasts lack a ruffled border and form no resorption lacunae (5). Thus, the predominant phenotype in mice lacking the *c-src* gene shows osteopetrosis resulting from defective ruffled borders in osteoclasts.

Both *c-fos*$^{-/-}$ and *c-src*$^{-/-}$mice can grow to the adult stage, revealing similar osteopetrotic feature, even though the reason of defective bone resorption is different — osteoclastic absence or dysfunctional osteoclasts for bone resorption. Therefore, in this study, we have histochemically examined the cellular activities of osteoblasts and osteoclasts in the femora of *c-fos*$^{-/-}$ and *c-src*$^{-/-}$ mice, in order to verify which of the different cellular circumstances, the presence of osteoclasts themselves or bone resorption by osteoclasts, is essential for cell coupling to osteoblastic activity.

MATERIALS AND METHODS

Tissue preparation for histochemistry and electron microscopy. Twelve-week old mice homozygous for gene depletion of *c-fos* or *c-src*, and the age-matched *wild-type* mice ($n = 6$ for each, The Jackson Laboratory, Inc., Bar Harbor, ME) were used. All animal experiments in this study were conducted under the Guidelines for Animal Experimentation of Hokkaido University (Approved No. # 15-0041). They were perfused with a fixative of 4% paraformaldehyde in a 0.1 M cacodylate buffer (pH 7.4) through the left ventricle under anesthesia using diethyl ether inhalation followed by an intraperitoneal injection of chloral hydrate. Femora and tibiae were removed *en bloc* and immediately immersed in the same fixative for 18 h. Femora were decalcified with 10% EDTA for 2 months prior to paraffin-embedding. Five μm-thick paraffin sections were cut sagittally and parallel to the bone longitudinal axis prior to routine hematoxylin and eosin staining and histochemistry as described below. All sections were photographed under a Nikon Eclipse E800 microscope (Nikon Instruments Inc. Tokyo, Japan), and light microscopic images were acquired with a digital camera (Nikon DXM1200C, Nikon).

For ultrastructural observation by transmission electron microscope (TEM), after perfusion of 4% paraformaldehyde solution, the extracted femora and tibiae were immediately immersed in a mixture containing 2% paraformaldehyde and 2.5% glutaraldehyde diluted in a 0.067 M cacodylate buffer (pH 7.4) for additional 18 h. Some specimens were decalcified with 5% EDTA for 2 months, while others were kept undecalcified. Both samples were then post-fixed in a mixture of 1% OsO_4 for 4 h, dehydrated with ascending concentrations of acetone, and then embedded in epoxy resin (Taab, Berkshire, UK). Ultrathin sections with 120 nm thickness were obtained by ultramicrotome (Sorvall MT-5000; Ivan Sorvall, Inc., Norwalk, CT). The sections of decalcified specimens were stained with uranyl acetate and lead citrate, while the ultrathin sections of undecalcified specimens were not stained prior to examination under a TEM (Hitachi H-7100; Hitachi Co. Ltd., Tokyo,

Japan) at an accelerating voltage of 80 kV.

Histochemical staining of TNALPase, TRAPase, osteopontin and EphB4/ephrinB2. Dewaxed paraffin sections were examined for tissue nonspecific alkaline phosphatase (TNALPase) as previously reported (1). In brief, the sections were immersed in methanol containing 0.3% H_2O_2 for 30 min to block endogenous peroxidase. To reduce non-specific binding, 1% bovine serum albumin (Seologicals Proteins Inc. Kankakee, IL) in PBS (1% BSA-PBS) was applied to the sections for 20 min. They were then incubated with rabbit polyclonal antiserum against TNALPase (27) at a dilution of 1 : 200 with 1% BSA-PBS at room temperature (RT) for 2 h. Following several washings in PBS, they were incubated with horseradish peroxidase (HRP)-conjugated anti-rabbit IgG (Chemicon International Inc., Temecula, CA) for 1 h. The sections were subsequently treated with 3,3'-diaminobenzidine tetrahydrochloride (DAB) to visualize the immunoreaction.

For detection of tartrate-resistant acid phosphatase (TRAPase) (3), the sections were incubated in a mixture of 8 mg of naphthol AS-BI phosphate (Sigma, St. Louis, MO), 70 mg of red violet LB salt (Sigma) and 50 mM L(+) tartaric acid (0.76 g; Nacalai Tesque, Kyoto, Japan) diluted in 0.1 M sodium acetate buffer (pH 5.0) for 20 min at 37°C.

For double detection of TNALPase and TRAPase, TNALPase immunostaining was performed prior to TRAPase enzyme histochemistry: Some sections were reacted with HRP-conjugated anti-rabbit IgG (Chemicon), or ALPase-conjugated anti-rabbit IgG (Sigma-Aldrich, Inc., St. Louis, MO), in which TNALPase activity was shown with a blue stain by means of enzymatic histochemistry. In brief, sections were immersed in a mixture of 6 mg of naphthol AS-BI phosphate (Sigma), 36 mg of fast blue RR salt (Sigma) diluted in 30 mL of 0.05 M Tris-HCl buffer (pH 9.0) for 10–15 min at RT.

As previously reported (2, 23), the detection of osteopontin was started with endogenous peroxidase inhibition for dewaxed sections. After pre-incubation with 1% BSA-PBS for 30 min at RT, the sections were incubated with rabbit polyclonal antisera against osteopontin (Cosmo Bio Co., Ltd., Tokyo, Japan) at 1 : 2000 for 1 h. The treated sections were then incubated with HRP-conjugated goat anti-rabbit IgG (Chemicon). For EphB4/ephrinB2 staining, the sections were incubated with goat anti-mouse EphB4 (R&D Systems, Minneapolis, MN) diluted at 1 : 50, or with goat anti-mouse ephrinB2 (R&D Systems) diluted at 1 : 25 for 2 h at RT, and then, incubated with HRP-conjugated anti-goat secondary antibody (Chemicon) for 1 h at RT. For visualization of all immunoreactions, DAB was employed as a substrate. All sections were counterstained with methyl green, and observed under light microscopy (Eclipse E800; Nikon Instruments Inc. Tokyo, Japan).

Von Kossa staining for detection of mineralized matrices. Von Kossa staining was performed as described previously (31, 32). Shortly, undecalcified semi-thin epoxy resin sections were incubated with an aqueous solution of 5% silver nitrate (Wako Pure Chemical Industries, Ltd, Osaka, Japan) for 60 min at RT under sunlight until they took on a dark brown color. Following a distilled water rinse, the sections were incubated with a 5% sodium thiosulfate solution (Wako Pure Chemical Industries) for 5 min. The sections were then, faintly stained with toluidine blue.

RESULTS

The distribution of osteoblasts, osteoclasts and cement lines in c-fos$^{-/-}$ and c-src$^{-/-}$ mice

Femora of 12-week old *wild-type* mice demonstrated many metaphyseal trabeculae parallel to the longitudinal axis and a broad bone marrow area (Fig. 1A). In contrast, the histological appearance of femora was similar between *c-fos*$^{-/-}$ and *c-src*$^{-/-}$ mice, forming abundant trabeculae occupying the area of bone marrow (Figs. 1B, C): The osteoclasts' absence and dysfunction on bone resorption resulted in the similar osteopetrotic feature. There were no TRAPase-reactive osteoclasts in *c-fos*$^{-/-}$ mice (compare Figs. 1D and 1E), while many TRAPase-reactive osteoclasts were seen in *c-src*$^{-/-}$ mice (Fig. 1F). Interestingly, many osteoblasts intensely positive for TNALPase were present throughout the *c-src*$^{-/-}$ femora (Fig. 1I), while *c-fos*$^{-/-}$ specimens showed only a few TNALPase-positive osteoblasts (compare Figs. 1G and 1H).

Another remarkable finding in *c-src*$^{-/-}$ mice was the parallel layer of TRAPase-reactive/osteopontin-positive cement lines in the superficial region of the bone matrix (Figs. 2A, 2B). In contrast, normal bone matrix of the *wild-type* counterparts did not show the parallel layers of TRAPase-reactive/osteopontin-positive cement lines (data not shown). In addition, an intense activity of TNALPase could be seen in osteoblasts in the matched areas (Fig. 2C), therefore, implying that the *c-src*$^{-/-}$ osteoblasts deposited new bone matrices onto the older ones. When observing at a higher magnification, intense

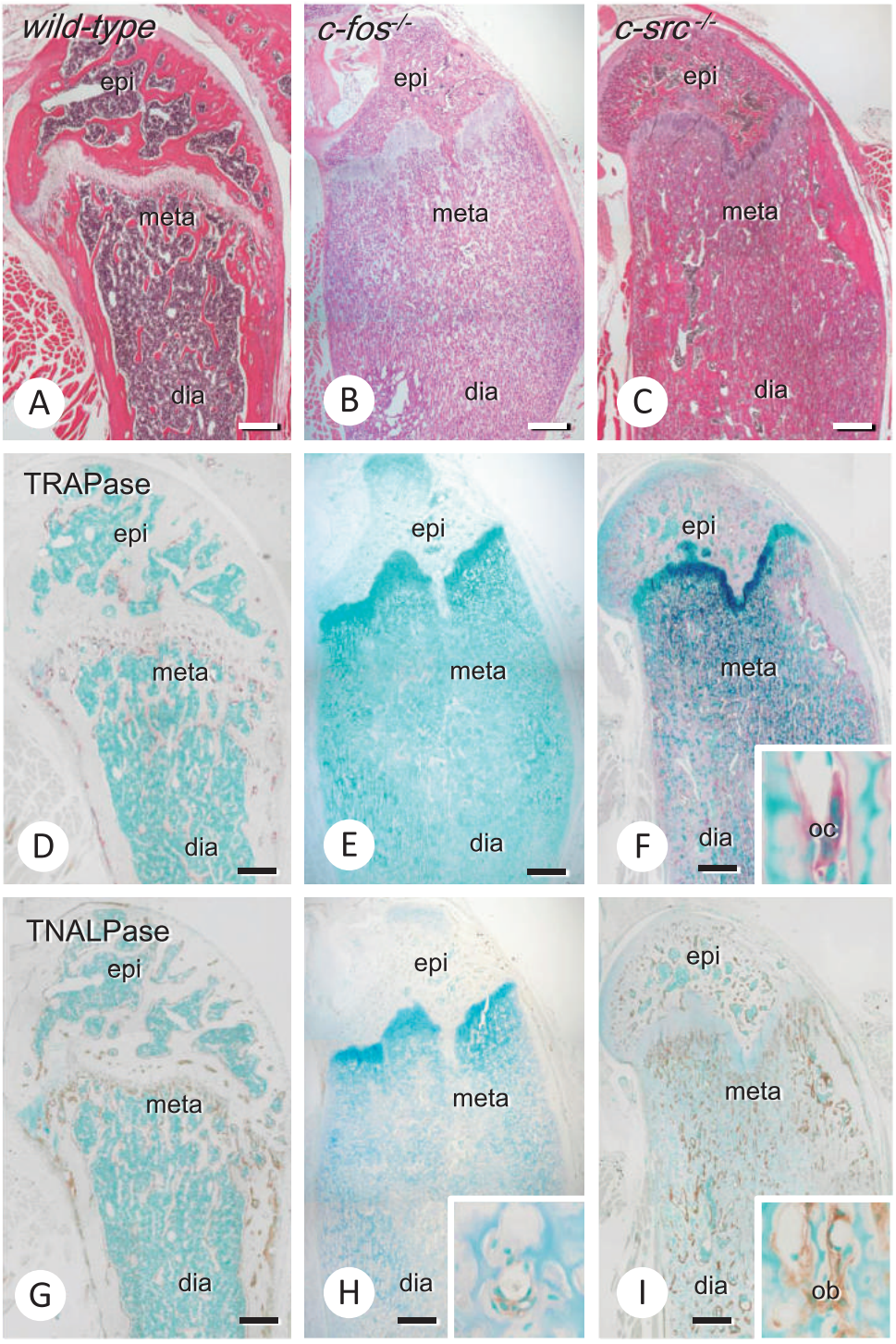

Fig. 1 The distribution of TRAPase-reactive osteoclasts and TNALPase-positive osteoblasts in *wild-type*, *c-fos*$^{-/-}$ and *c-src*$^{-/-}$ femora. The *wild-type* femur (A) shows the distinct regions of metaphysis (meta) and diaphysis (dia) with bone marrow tissue, while *c-fos*$^{-/-}$ (B) and *c-src*$^{-/-}$ (C) femora develop abundant trabeculae throughout metaphyses and diaphyses. There are a large numbers of TRAPase-positive dots indicative of osteoclasts (red color) in the *wild-type* mice (D) and *c-src*$^{-/-}$ mice (F). An inset of panel F shows a higher magnified image of metaphysis, featuring a TRAPase-reactive osteoclast (oc). Note no TRAPase-positivity in *c-fos*$^{-/-}$ femur (E). Many TNALPase-reactive areas, *i.e.,* osteoblasts (brown color) are seen in both the *wild-type* (G) and *c-src*$^{-/-}$ femora (I). An inset of panel I displays TNALPase-positive osteoblasts (ob) in *c-src*$^{-/-}$ femora. However, *c-fos*$^{-/-}$ specimens hardly showed TNALPase-reactivity (H). An inset of Panel H shows weak TNALPase-positivity (faint brown). epi: epiphysis, Bars, A–I: 300 μm

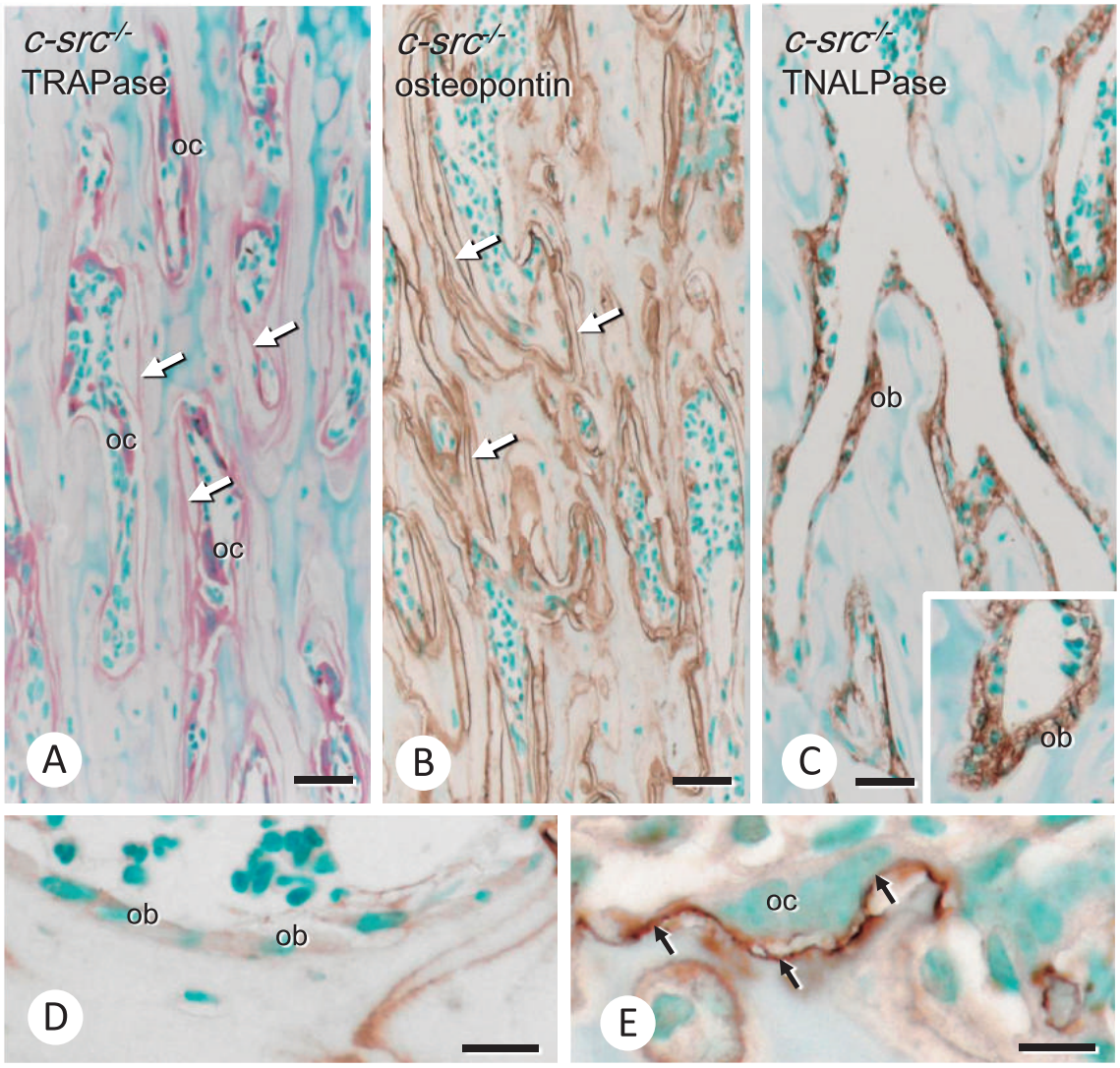

Fig. 2 TRAPase-reactive/osteopontin-positive cement lines in *c-src*$^{-/-}$ bone. *c-src*$^{-/-}$ mice demonstrate not only TRAPase-reactive osteoclasts (oc, red color), but also parallel layers of TRAPase-reactive cement lines (arrows, red lines) in the superficial region of the bone matrix (A). In the corresponding region, such cement lines are also immunoreactive for osteopontin (arrows, brown color), revealing the parallel layers (B). *c-src*$^{-/-}$ osteoblasts (ob) show an intense activity of TNALPase (brown) in the matched region (C). An inset in panel C reveals higher magnification of TNALPase-reactive *c-src*$^{-/-}$osteoblasts. There is a very faint reactivity of osteopontin adjacent to osteoblasts (ob, D), but an intense osteopontin immunoreactivity (arrows, brown) beneath the *c-src*$^{-/-}$ osteoclasts (oc, E). Bars, A–C: 30 μm, D, E: 10 μm

osteopontin-immunoreactivity was seen beneath the *c-src*$^{-/-}$ osteoclasts rather than osteoblasts, indicating abundant osteopontin secreted from the osteoclasts (Figs. 2D, E). Taken together, it seems likely that osteoclasts passed along the bone surface without bone resorption, secreting TRAPase and osteopontin, and then, osteoblasts deposited new bone matrices onto the bone surfaces in *c-src*$^{-/-}$ mice. Such parallel layers of TRAPase-reactive/osteopontin-positive cement lines were not observed in *c-fos*$^{-/-}$ mice (data not shown).

Ultrastructures of osteoblasts and osteoclasts in c-fos$^{-/-}$ *and c-src*$^{-/-}$ *mice*

We next examined the ultrastructures of osteoblasts and osteoclasts under TEM. *Wild-type* mice demonstrated a typical feature of mature osteoblasts with well-developed rough endoplasmic reticulum (rER) and assemblies of Golgi apparatus (Fig. 3A). In contrast, *c-fos*$^{-/-}$ bone revealed only a few osteoblastic cells located on the bone surface, which did not developed rER and Golgi apparatus. The osteoblastic cells located on *c-fos*$^{-/-}$ bone have been previous-

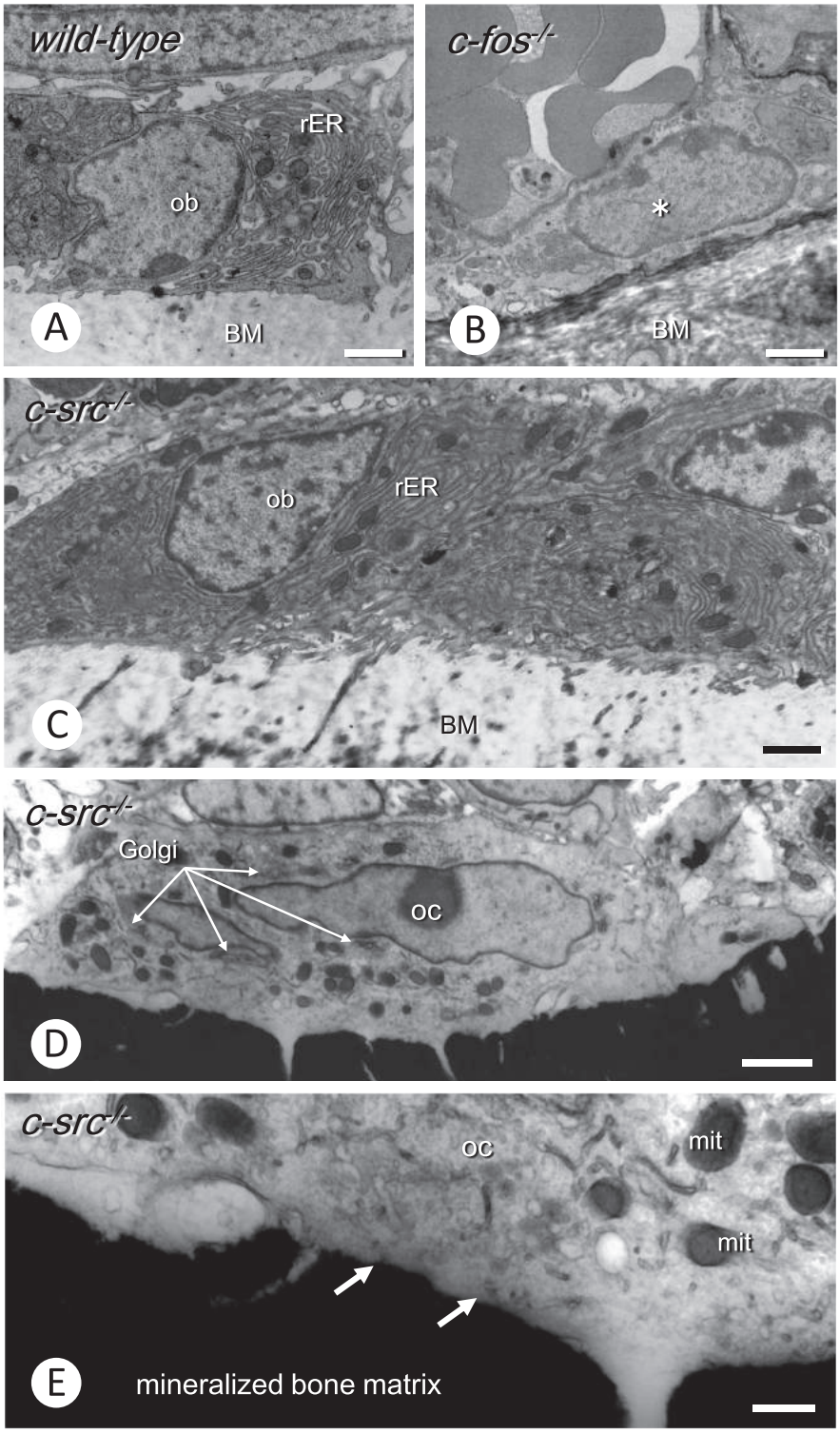

Fig. 3 Ultrastructures of osteoblasts and osteoclasts in *c-fos*$^{-/-}$ and *c-src*$^{-/-}$ mice. TEM observations demonstrate plump osteoblasts (ob) with well-developed rough endoplasmic reticulum (rER) in the *wild-type* mice (A), whereas *c-fos*$^{-/-}$ bone reveals somehow flattened cells (an asterisk) with poorly-developed rER (B). *c-src*$^{-/-}$ mice showed many mature osteoblasts (ob) containing well-developed rER (C). Panels D and E are TEM observations of *c-src*$^{-/-}$ osteoclasts (oc) in and undemineralized specimens. A *c-src*$^{-/-}$ osteoclast lacks typical ruffled borders and clear zone, showing only a few vacuoles and vesicles (D). This osteoclast attaches the bone surface with its cell body (arrows, E). Note Golgi apparatus (Golgi, D) surrounding nuclei and relatively-abundant mitochondria (mit, E). BM: bone matrix, Bars, A–D: 2 μm, E: 0.5 μm

ly suggested as osteoblastic precursors rather than mature osteoblasts (21) (Fig. 3B). Like *wild-type* mice, however, c-*src*$^{-/-}$ mice showed many mature osteoblasts possessing well-developed rER and Golgi apparatus (Fig. 3C). Using undecalcified ultrathin sections, *c-src*$^{-/-}$ osteoclasts were shown not to develop ruffled border, highly folded cell membrane facing the underlying bone surface, nor to erode mineralized bone matrices (Figs. 3D, 3E).

Ultrastructural findings of cell-to-cell contacts with osteoclasts and osteoblasts, and mineralized bone formation in in c-src$^{-/-}$ *mice*

Light microscopic observation on semi-thin sections demonstrated mature osteoblasts in the close proximity of osteoclasts located on osteoid in *c-src*$^{-/-}$ mice (Fig. 4A). There could be seen linear structures identical to cement lines and osteocytes inside the bone matrix. Consistently, histochemical assessment verified TNALPase-positive osteoblasts which were localized adjacent to TRAPase-reactive osteoclasts on the *c-src*$^{-/-}$ bone surface (Figs. 4B, 4C). TEM observation further demonstrated that mature cuboidal osteoblasts featuring developed rER made cell-to-cell-contact with osteoclasts by means of their cytoplasmic processes, and these mature osteoblasts were localized on osteoid in which many mineralized nodules can be seen (Fig. 4D).

We attempted to examine bone mineralization between the *wild-type* and *c-src*$^{-/-}$ mice, since cell coupling may facilitate osteoblasts to deposit mineralized bone matrices if cell coupling works in the *c-src*$^{-/-}$ bone. As a consequence, like *wild-type* mice (Figs. 5A–C), well-mineralized bone matrix stained with von Kossa method was observed in *c-src*$^{-/-}$ mice (Figs. 5D–F), and incompletely-mineralized osteoid was discernible, implying normally-mineralized bone matrix (Fig. 5F).

Immnolocalization of ephrinB2 and EphB4 in c-fos$^{-/-}$ *and c-src*$^{-/-}$*mice*

The binding of ephrinB2 and EphB4 was previously reported as a candidate for cell coupling between osteoclasts and osteoblasts (21, 41). Both immunoreactivities of EphB4 and ephrinB2 were seen mainly on endothelial cells in the *c-fos*$^{-/-}$ mice (Figs. 6A, B). No osteoblastic cells seemed to show EphB4, and there were no osteoclasts in *c-fos*$^{-/-}$ bone. In contrast, in *c-src*$^{-/-}$ bone, EphB4-reactivity was seen mainly in osteoblastic cells and slightly in endothelial cells of blood vessels, while ephrinB2-positivity was discernible in both osteoclasts and endothelial cells (Figs. 6C, D). In both *c-fos*$^{-/-}$ and *c-src*$^{-/-}$ mice, osteocytes and bone marrow cells did not exhibit any immunoreactivities of EphB4 and ephrinB2.

DISCUSSION

To our knowledge, this is the first report to attempt to histologically demonstrate which of the two cellular circumstances, the presence of osteoclasts themselves or bone resorption by osteoclasts, is essential for subsequent osteoblastic activity *in vivo*. We have observed several histological findings concerning osteoblastic activation in *c-src*$^{-/-}$ mice. Unlike *c-fos*$^{-/-}$ mice, *c-src*$^{-/-}$ mice revealed osteoblasts intensely positive for TNALPase, and also demonstrated the parallel layers of cement lines in the superficial bone matrix, indicating that the new bones were piled up to older bone. In addition, osteoblasts made cell-to-cell contacts with osteoclasts, developed abundant rER and Golgi apparatus, and had deposited osteoid in *c-src*$^{-/-}$ mice. Thus, *c-src*$^{-/-}$ mice showed more active osteoblasts than *c-fos*$^{-/-}$ mice did, and the presence of osteoclasts even with a lack of ruffled borders seems to make osteoblasts active. Taken together, we propose the possibility that the presence of osteoclasts themselves, rather than osteoclastic bone resorption, is important for subsequent activation of osteoblasts during bone remodeling.

In the cellular process of bone remodeling, osteoclastic bone resorption precedes osteoblastic bone formation. In the formation phase of physiological bone remodeling (4, 10, 11, 13), osteoblasts would be activated to migrate onto the once-resorbed bone surface, and secrete bone matrices (4, 39). Such cellular sequence in bone remodeling is strictly maintained, so that we assume that after bone resorption, osteoclasts communicate and activate surrounding osteoblastic cells. Our own observation in this study can support the hypothesis of a "coupling factor" predicted by Howard *et al.* (17), and postulate that coupling factors would be derived from osteoclasts, but the bone remodeling is not achieved by any growth factors released from bone matrix—TGFβ or IGFs which had been embedded in bone by osteoblasts and would be released by osteoclastic bone resorption (7, 15, 16).

One may wonder why despite defective bone remodeling, *c-fos*$^{-/-}$ femora and tibiae can longitudinally grow to the similar length as the *wild-type* phenotype. Unlike bone remodeling, in the modeling area of growing bone, *i.e.,* endochondral ossification at chondro-osseous junction, osteoblastic activity may be regulated in different ways. We noticed that

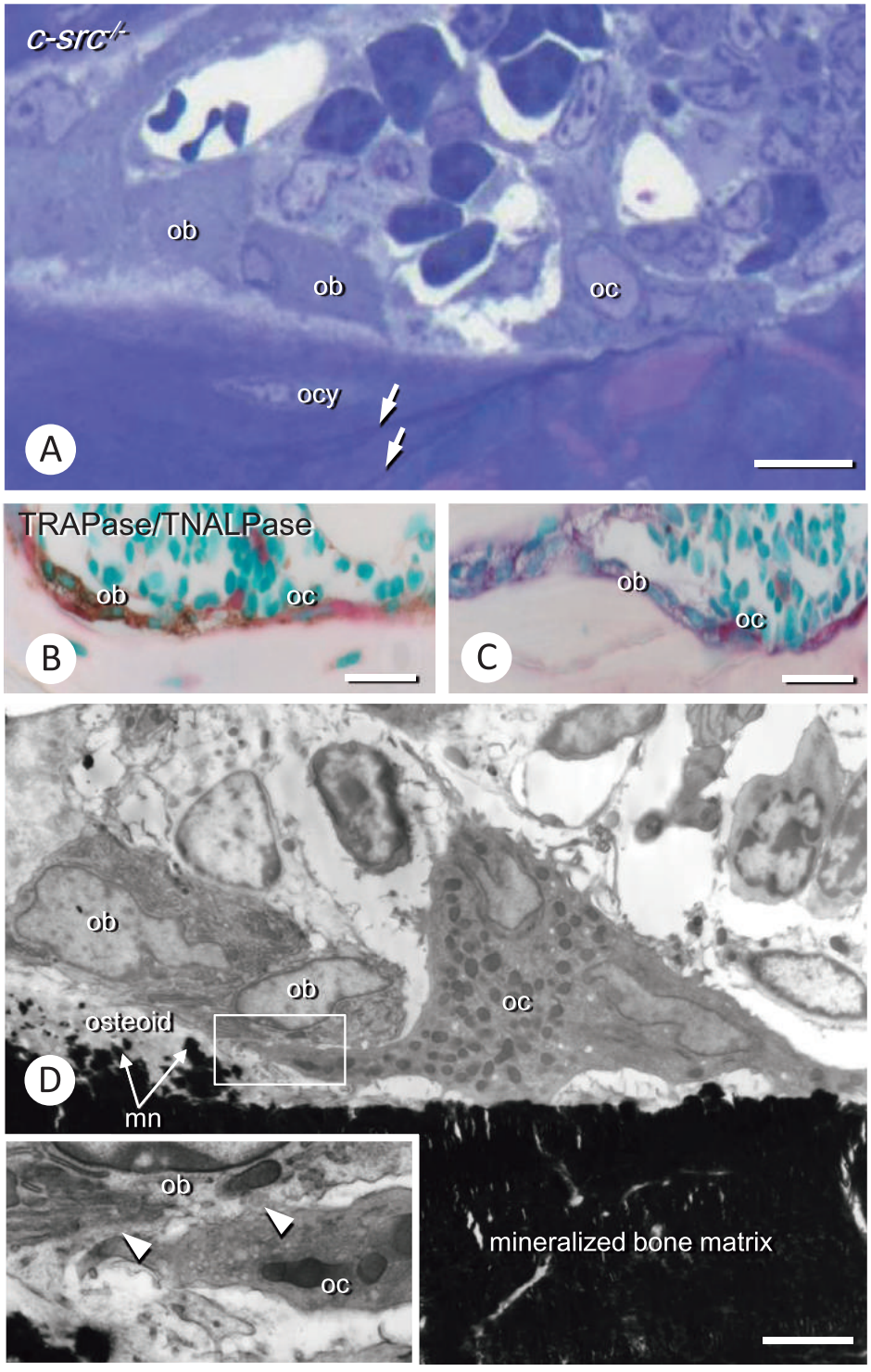

Fig. 4 Histological findings on cellular interaction between osteoclasts and osteoblasts in *c-src*$^{-/-}$ mice. A semi-thin section shows mature osteoblasts (ob) in the close proximity of an osteoclast (oc) (A). Note an osteocyte (ocy) and cement lines (white arrows) extending from beneath the osteoclast to the deeper portion (A). Combined detection for TNALPase immunohistochemistry and TRAPase enzyme histochemistry (B, C) displays neighboring osteoclasts (oc, red) and osteoblasts (ob, brown in B, blue in C). TEM observation of the matched region of panel A displays mature cuboidal osteoblasts (ob) featuring a cell-to-cell contact to the neighboring osteoclast (oc) with their cytoplasmic processes (D). Note osteoid beneath the osteoblasts (ob), which includes mineralized nodules (mn). An inset of panel D shows a direct contact (arrowheads) of cytoplasmic processes of neighboring osteoblasts and the osteoclast. Bars, A: 5 μm, B, C: 10 μm, D: 3 μm

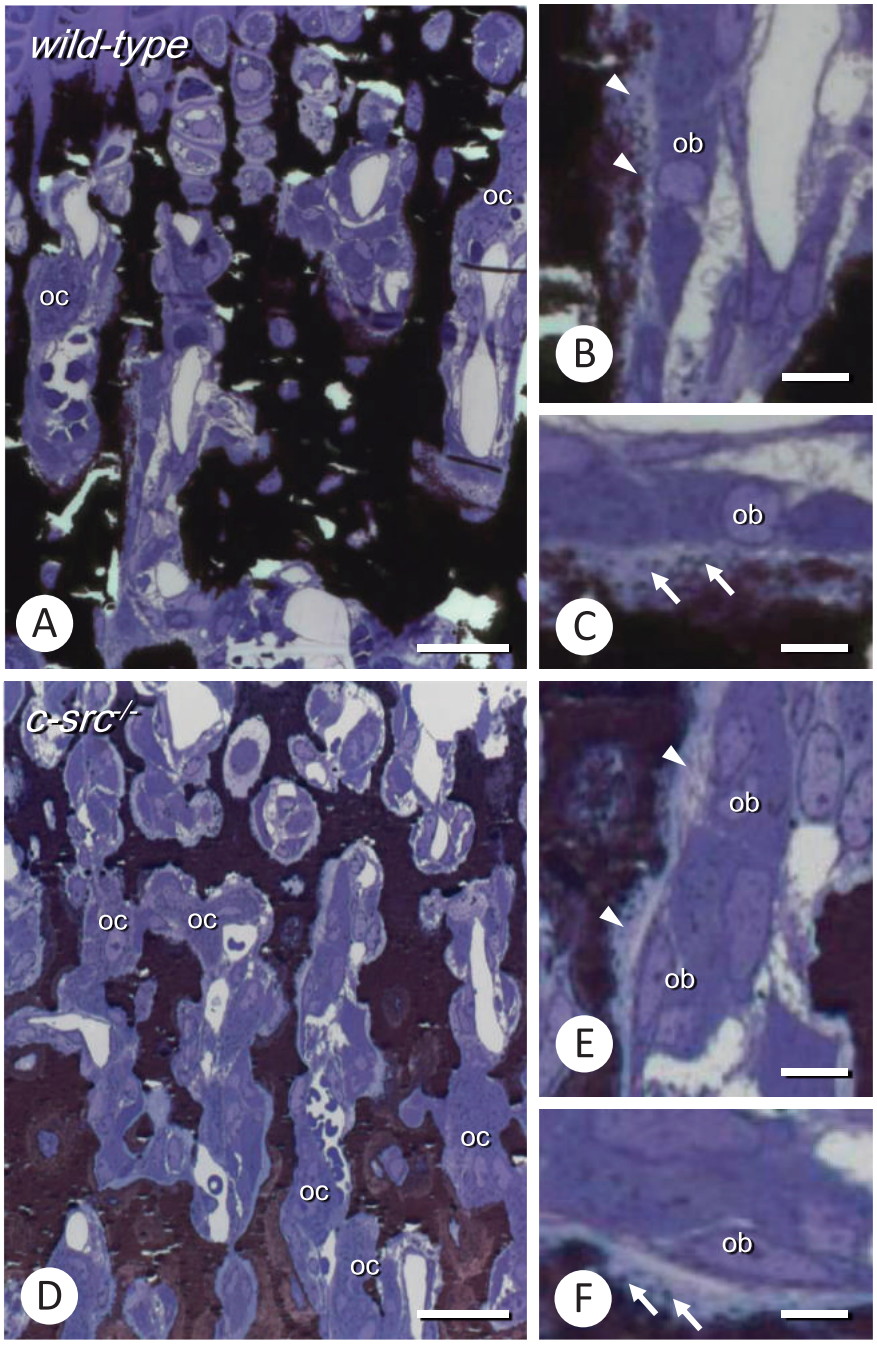

Fig. 5 Von Kossa staining of metaphyseal trabeculae of *wild-type* and *c-src*$^{-/-}$ mice. Von Kossa staining visualizes mineralization (dark brown color) of the *wild-type* (A–C) and *c-src*$^{-/-}$ (D–F) bone. The *wild-type* trabeculae is well-mineralized (dark brown) stained by von Kossa's method (A), and demonstrate the osteoid (arrowheads, B) with featuring mineralized granular structures identical to mineralized nodules (arrows, C). Consistently, *c-src*$^{-/-}$ mice develop well-mineralized trabeculae despite of many osteoclasts (oc, D). At higher magnifications, incompletely-mineralized osteoid (arrowheads, E) can be seen beneath cuboidal osteoblasts (ob, E). Note granular structures indicative of mineralized nodules (arrows, F). Bars, A, C: 20 μm, B, D: 3 μm

osteoblasts close to the chondro-osseous junction were activated even in the deficiency of *c-fos* gene (data not shown). Although the spatial arrangement of trabeculae is distorted, *c-fos*$^{-/-}$ bone can therefore elongate as the *wild-type* counterpart. Thus, we should distinguish the cellular and molecular mech-

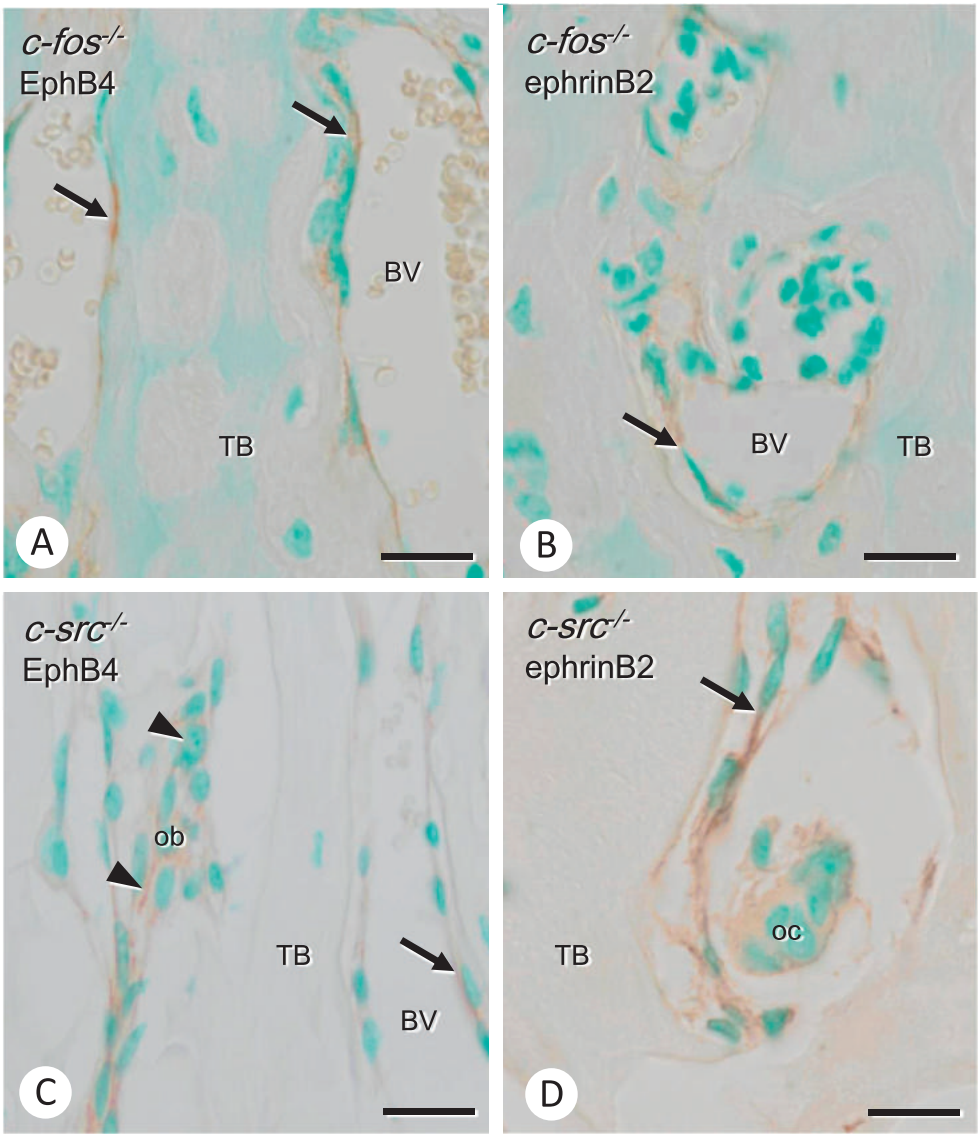

Fig. 6 Immnolocalization of EphB4 and ephrinB2 in *c-fos*$^{-/-}$ and *c-src*$^{-/-}$ mice. In the *c-fos*$^{-/-}$ mice, the immunoreactivities of EphB4 and ephrinB2 (brown color) are seen mainly on endothelial cells (arrows) in panels A and B, respectively. In contrast, in *c-src*$^{-/-}$ mice, EphB4-reactivity (arrowheads, brown) is observed mainly in osteoblastic cells (ob) and slight on the endothelial cells (an arrow) as shown in panel C. EphrinB2-positivity (brown) can be seen in both an osteoclast (oc) and endothelial cells (an arrow) in panel D. TB: trabecular bone, BV: blood vessel, Bars, A–D: 10 μm

anism on bone formation between modeling and remodeling sites.

In contrast to the modeling site, the bone remodeling sites such as secondary trabeculae appear to need cell coupling between osteoclasts and osteoblasts, since the defective coupling due to the osteoclastic absence in the *c-fos*$^{-/-}$ mice resulted in markedly-reduced activity of osteoblasts in the areas of secondary trabeculae. It is previously suggested that *fos* ablation does not seem to affect osteoblastic differentiation *in vitro*: calvarial cells derived from mice heterozygous and homozygous for *c-fos* deletion did not seem to be compromised in their differentiation (20). This means that the potential cellular activity of osteoblasts itself is not diminished in *c-fos* deficiency, and therefore, the presence of osteoclasts seems to affect the osteoblastic activities in bone remodeling sites *in vivo*. We have previously reported that cell coupling with osteoclasts *in vivo* is necessary for preosteoblastic differentiation into mature osteoblasts to deposit new bone in response to parathyroid hormone (21). Consistently, *op/op* mice, an-

other mouse model lacking osteoclasts (9, 18, 19, 22) revealed the extremely-reduced osteoblastic activity in long bones (26), and defective bone mineralization (30). Taken together, the presence of osteoclasts is important for cell coupling to activate osteoblastic cells in bone remodeling sites *in vivo*.

Three cellular manners can be assumed regarding how coupling factors would be provided from osteoclasts to osteoblasts; first, membrane-bound coupling factors might be provided to osteoblasts by cell-to-cell contacts; second, coupling factors might be secreted from osteoclasts, affecting the surrounding osteoblastic cells; and third, coupling factors previously embedded in bone matrix might be released by osteoclastic bone resorption. Several reports have documented the occurrence of cell-to-cell contacts between osteoclastic precursors and osteoblastic cells during osteoclastic differentiation (3, 35–37). However, in turn, the cell-to-cell contact may allow the signaling from osteoclasts to osteoblastic cells. As shown in Figs. 2 and 4, *c-src*$^{-/-}$ mice demonstrated mature osteoblasts featuring cell-to-cell contacts with neighboring osteoclasts, and revealed TRAPase-reactive/osteopontin-positive cement lines parallely localized in the bone matrix. This implicates that once *c-src*$^{-/-}$ osteoclasts pass along the bone surface without resorbing bone, activated osteoblasts would deposit new bone matrices on the bone surface, forming the piled up layers of bone matrices. Thus, we hypothesize the possibility that cell-to-cell contact, at least in part, is intrinsic for cell coupling between osteoclasts and osteoblastic cells.

Alternatively, local coupling factors linking bone resorption to subsequent formation have long been proposed as the key regulator of the bone remodeling process. TGFβ and IGF-1 (7, 15, 16) were postulated to function as a coupling factor, but during the decade, more candidates were raised—complement component 3a (24), matrix IGF-1 (6), E-secletin ligand 1 (40), integrated actions of c-Src, IL-6 and IGFBP5 (28), semaphorin 3A (14), and Dlx5 (29). Among these molecules, we postulated that EphB4/ephrinB2 (41) would behave as coupling factors as reported previously (21). In our study, ephrinB2 was faintly seen in osteoclasts, while EphB4 was observed in osteoblasts. Non-resorbing osteoclasts can bind ephrinB2 to osteoblastic EphB4 for activating them. However, the coupling factors may not be the sole molecule, but must be a complex of a variety of molecules. Therefore, further investigation seems to be necessary for identifying coupling factors.

In conclusion, unlike *c-fos*$^{-/-}$ mice, *c-src*$^{-/-}$ mice demonstrated activated, mature osteoblasts, and parallel layers of cement lines in the superficial bone matrix, indicating the new bones were piled up to older bone. Therefore, cellular circumstance with dysfunctional osteoclasts but not osteoclastic absence is able to activate osteoblasts, which indicate that osteoclastic presence is essential for cell coupling to osteoblasts.

Acknowledgements

This study was partially supported by the Grants-in Aid for Scientific Research (Amizuka N, Hasegawa T) and Promoting International Joint Research (Bilateral Collaborations) of JSPS and NSFC (Amizuka N, Li M).

DISCLOSURES

The authors have no financial conflicts of interest.

REFERENCES

1. Amizuka N, Kwan M, Goltzman D, Ozawa H and White JH (1999) Vitamin D_3 differentially regulates parathyroid hormone/parathyroid hormone-related peptide receptor expression in bone and cartilage. *J Clin Invest* **103**, 373–381.
2. Amizuka N, Li M, Hara K, Kobayashi M, de Freitas PH, Ubaidus, Oda K and Akiyama Y (2009) Warfarin administration disrupts the assembly of mineralized nodules in the osteoid. *J Electron Microsc* **58**, 55–65.
3. Amizuka N, Takahashi N, Udagawa N, Suda T and Ozawa H (1997) An ultrastructural study of cell-cell contact between mouse spleen cells and calvaria-derived osteoblastic cells in a co-culture system for psteoclast formation. *Acta Histochem Cytochem* **30**, 351–362.
4. Baron R, Vignery A and Horowits M (1983) Lymphocytes, macrophages and the regulation of bone remodeling. In: *Bone and Mineral Research*, Annual **2** (Peck WA, ed.), pp175–243, Elservier Science, New York.
5. Boyce BF, Yoneda T, Lowe C, Soriano P and Mundy GR (1992) Requirement of pp60c-src expression for osteoclasts to form ruffled borders and resorb bone in mice. *J Clin Invest* **90**, 1622–1627.
6. Crane JL and Cao X (2014) Function of matrix IGF-1 in coupling bone resorption and formation. *J Mol Med (Berl)* **92**, 107–115.
7. Erlebacher A, Filvaroff EH, Ye JQ and Derynck R (1998) Osteoblastic responses to TGF-beta during bone remodeling. *Mol Biol Cell* **9**, 1903–1918.
8. Felix R, Hofstetter W and Cecchini MG (1996) Recent developments in the understanding of the pathophysiology of osteopetrosis. *Eur J Endocrinol* **134**, 143–156.
9. Felix R, Cecchini MG and Fleisch H (1990) Macrophage colony-stimulating factor restores in vivo bone resorption in the op/op mouse. *Endocrinology* **127**, 2592–2594.
10. Frost, HM (1964) Dynamics of bone remodeling. In: *Bone Biodynamics* (Frost HM, ed.), pp.315–333, Little, Brown, Boston.

11. Frost HM (1969) Tetracycline-based histological analysis of bone remodeling. *Calcif Tissue Res* **3**, 211–237.
12. Grigoriadis AE, Wang ZQ, Cecchini MG, Hofstetter W, Felix R, Fleisch HA and Wagner EF (1994) c-Fos: a key regulator of osteoclast-macrophage lineage determination and bone remodeling. *Science* **266**, 443–448.
13. Hattner R, Epker BN and Frost HM (1965) Suggested sequential mode of control of changes in cell behaviour in adult bone remodelling. *Nature* **206**, 489–490.
14. Hayashi M, Nakashima T, Taniguchi M, Kodama T, Kumanogoh A and Takayanagi H (2012) Osteoprotection by semaphorin 3A. *Nature* **485**, 69–74.
15. Hayden JM, Mohan S and Baylink DJ (1995) The insulin-like growth factor system and the coupling of formation to resorption. *Bone* **17**, 93S–98S.
16. Horner A, Kemp P, Summers C, Bord S, Bishop NJ, Kelsall AW, Coleman N and Compston JE (1998) Expression and distribution of transforming growth factor-beta isoforms and their signaling receptors in growing human bone. *Bone* **23**, 95–102.
17. Howard GA, Bottemiller BL, Turner RT, Rader JI and Baylink DJ (1998) Parathyroid hormon stimulates bone formation and resorption in organ culture: evidence for a coupling mechanism. *Proc Natl Acad Sci USA* **78**, 3204–3208.
18. Kodama H, Nose M, Niida S and Yamasaki A (1991) Essential role of macrophage colony-stimulating factor in the osteoclast differentiation supported by stromal cells. *J Exp Med* **173**, 1291–1294.
19. Kodama H, Yamasaki A, Nose M, Niida S, Ohgame Y, Abe M, Kumegawa M and Suda T (1991) Congenital osteoclast deficiency in osteopetrotic (op/op) mice in cured by injections of macrophage colony-stimulating factor. *J Exp Med* **173**, 269–272.
20. Koh AJ, Demiralp B, Neiva KG, Hooten J, Nohutcu RM, Shim H, Datta NS, Taichman RS and McCauley LK (2005) Cells of the osteoclast lineage as mediators of the anabolic actions of parathyroid hormone in bone. *Endocrinology* **146**, 4584–4596.
21. Luiz de Freitas PH, Li M, Ninomiya T, Nakamura M, Ubaidus S, Oda K, Udagawa N, Maeda T, Takagi R and Amizuka N (2009) Intermittent PTH administration stimulates pre-osteoblastic proliferation without leading to enhanced bone formation in osteoclast-less c-fos(−/−) mice. *J Bone Miner Res* **24**, 1586–1597.
22. Marks SC Jr (1982) Morphological evidence of reduced bone resorption in osteopetrotic (op) mouse. *J Anat* **163**, 157–167.
23. Masuki H, Li M, Hasegawa T, Suzuki R, Ying G, Zhusheng L, Oda K, Yamamoto T, Kawanami M and Amizuka N (2010) Immunolocalization of DMP1 and sclerostin in the epiphyseal trabecule and diaphyseal cortical bone of osteoprotegerin deficient mice. *Biomed Res (Tokyo)* **31**, 307–318.
24. Matsuoka K, Park KA, Ito M, Ikeda K and Takeshita S (2014) Osteoclast-derived complement component 3a stimulates osteoblast differentiation. *J Bone Miner Res* **29**, 1522–1530.
25. Miyazaki T, Tanaka S, Sanjay A and Baron R (2006) The role of c-Src kinase in the regulation of osteoclast function. *Mod Rheumatol* **16**, 68–74.
26. Nishino I, Amizuka N and Ozawa H (2001) Histochemical examination on osteoblastic activity in op/op mice with or without the injection of recombinant M-CSF. *J Bone Miner Metab* **19**, 267–276.
27. Oda K, Amaya Y, Fukushi-Irie M, Kinameri Y, Ohsuye K, Kubota I, Fujimura S and Kobayashi J (1999) A general method for rapid purification of soluble versions of glycosylphosphatidylinositol-anchored proteins expressed in insect cells: An application for human tissue-nonspecific alkaline phosphatase. *J Biochem* **126**, 694–699.
28. Peruzzi B, Cappariello A, Del Fattore A, Rucci N, De Benedetti F and Teti A (2010) c-Src and IL-6 inhibit osteoblast differentiation and integrate IGFBP5 signalling. *Nat Commun* **3**, 630. doi:10.1038/ncomms1651
29. Samee N, Geoffroy V, Marty C, Schiltz C, Vieux-Rochas M, Levi G and de Vernejoul MC (2008) Dlx5, a positive regulator of osteoblastogenesis, is essential for osteoblast-osteoclast coupling. *Am J Pathol* **173**, 773–780.
30. Sakagami N, Amizuka N, Li M, Takeuchi K, Hoshino M, Nakamura M, Nozawa-Inoue K, Udagawa N and Maeda T (2005) Reduced osteoblastic population and defective mineralization in osteopetrotic (op/op) mice. *Micron* **36**, 688–695.
31. Sasaki T, Amizuka N, Irie K, Ejiri S and Ozawa H (2000) Localization of alkaline phosphatase and osteopontin during mineralization in developing cartilage of caudal vertebrae. *Arch Histol Cytol* **63**, 271–284.
32. Sasaki M, Hasegawa T, Yamada T, Hongo H, de Freitas PH, Suzuki R, Yamamoto T, Tabata C, Toyosawa S, Yamamoto T, Oda K, Li M, Inoue N and Amizuka N (2013) Altered distribution of bone matrix proteins and defective bone mineralization in klotho-deficient mice. *Bone* **57**, 206–219.
33. Shaulian E and Karin M (2002) AP-1 as a regulator of cell life and death. *Nat Cell Biol* **4**, E131–E136.
34. Soriano P, Montgomery C, Geske R and Bradley A (1991) Targeted disruption of the c-src proto-oncogene leads to osteopetrosis in mice. *Cell* **64**, 693–702.
35. Takahashi N, Akatsu T, Udagawa N, Sasaki T, Yamaguchi A, Moseley JM, Martin TJ and Suda T (1988) Osteoblastic cells are involved in osteoclast formation. *Endocrinology* **23**, 2600–2602.
36. Takahashi N, Udagawa N, Akatsu T, Tanaka H, Isogai Y and Suda T (1991) Deficiency of osteoclasts in osteopetrotic mice is due to a defect in the local microenvironment provided by osteoblastic cells. *Endocrinology* **128**, 1792–1796.
37. Udagawa N, Takahashi N, Akatsu T, Sasaki T, Yamaguchi A, Kodama H, Martin TJ and Suda T (1989) The bone marrow-derived stromal cell lines MC3T3-G2/PA6 and ST2 support osteoclast-like cell differentiation in cocultures with mouse spleen cells. *Endocrinology* **125**, 1805–1813.
38. Wang ZQ, Ovitt C, Grigoriadis AE, Mohle-Steinlein U, Ruther U and Wagner EF (1992) Bone and haematopoietic defects in mice lacking c-fos. *Nature* **360**, 741–745.
39. Wergedal J and Baylink DJ (1969) Distribution of acid and alkaline phosphatase activity in undemineralized sections of the rat tibial diaphysis. *J Histochem Cytochem* **17**, 799–806.
40. Yang T, Grafe I, Bae Y, Chen S, Chen Y, Bertin TK, Jiang MM, Ambrose CG and Lee B (2013) E-selectin ligand 1 regulates bone remodeling by limiting bioactive TGF-β in the bone microenvironment. *Proc Natl Acad Sci USA* **110**, 7336–7341.
41. Zhao C, Irie N, Takada Y, Shimoda K, Miyamoto T, Nishiwaki T, Suda T and Matsuo K (2006) Bidirectional ephrinB2-EphB4 signaling controls bone homeostasis. *Cell Metab* **4**, 111–121.